JGR Space Physics

RESEARCH ARTICLE
10.1029/2025JA034916

# Influence of Diurnal Tide on the Low-Latitude UMLT Mean Zonal Wind: Evidence From Momentum Flux Estimation Using ICON/MIGHTI Winds

**Samadrita Basu[1,2], S. Sridharan[1], and J. Solomon Ivan[2]**

[1]National Atmospheric Research Laboratory, Pakala Mandal, Andhra Pradesh, India, [2]Indian Institute of Space Science and Technology, Thiruvananthapuram, Kerala, India

**Key Points:**

- Diurnal tide in meridional wind closely follows the seasonal variation of mean zonal wind in the low-latitude upper mesosphere and lower thermosphere (UMLT) region
- The momentum flux contributed by the diurnal tide is estimated and it is found to be found in the range 18–55 m/s/day
- Both vertical gradient of meridional flux of zonal momentum and convergence of vertical flux of zonal momentum are vital in modulating the MSAO of mean zonal winds

**Correspondence to:**
S. Sridharan,
susridharan@narl.gov.in

**Citation:**
Basu, S., Sridharan, S., & Ivan, J. S. (2026). Influence of diurnal tide on the low-latitude UMLT mean zonal wind: Evidence from momentum flux estimation using ICON/MIGHTI winds. *Journal of Geophysical Research: Space Physics*, *131*, e2025JA034916. https://doi.org/10.1029/2025JA034916

Received 28 NOV 2025
Accepted 28 MAR 2026

**Abstract** The influence of migrating diurnal tides in driving the mean zonal wind in the upper mesosphere and lower thermosphere (UMLT) is investigated using the zonal and meridional winds observed by the Michelson Interferometer for Global High-Resolution Thermospheric Imaging (MIGHTI) instrument onboard the Ionospheric Connection Explorer (ICON) satellite over the region of interest having a latitudinal and longitudinal extent of 5°N–15°N and 67.5°E–90°E, respectively, for the years 2020, 2021, and 2022. The mean zonal wind exhibits a distinct semiannual oscillation (SAO) with large westward winds found during January–March and September–December, varying in intensity (20–40 m/s) across all three years from 91 to 103 km. The diurnal tidal amplitude in meridional wind (DTV) reported equinoctial maximum (~80–100 m/s) and solstitial minimum (~10–30 m/s), revealing similar SAO found in mean zonal wind. The seasonal variation of westward acceleration, induced by the vertical gradient of meridional flux of zonal momentum ($F_{\text{meridional}}$), peaks during January-March (18–43 m/s/day) and September-December (40–55 m/s/day), exhibiting an equinoctial enhancement analogous to the westward wind intensity in mesospheric SAO. This quantitatively demonstrates the significance of momentum flux deposition by diurnal tides in driving the MSAO above 91 km using ICON/MIGHTI wind observations for the first time. The magnitude of westward acceleration (m/s/day) induced by $F_{\text{meridional}}$ exceeds the convergence of vertical flux of zonal momentum ($F_{\text{zonal}}$) due to diurnal tides from January to March, while the westward acceleration induced by both $F_{\text{zonal}}$ and $F_{\text{meridional}}$ are found to be larger and comparable during September–December.

**Plain Language Summary** The mean zonal wind in the upper mesosphere and lower thermosphere (UMLT) region exhibits semiannual variation with strong westward winds during equinox months and there is also an equinoctial asymmetry with large westward winds in one equinox compared to the other. Diurnal tide in meridional wind also shows similar variation with large amplitudes during the equinox months depicting similar equinoctial asymmetry. It is suggested that the diurnal tide, being the largest westward momentum source, contributes to the westward phase of semiannual variation as well as equinoctial asymmetry. The momentum flux contributed by the diurnal tide is also estimated and found to be in the range 18–55 m/s/day. The westward acceleration induced by the vertical gradient of meridional flux of zonal momentum due to diurnal tide exceeds the convergence of vertical flux of zonal momentum due to diurnal tide during January–March, while the westward acceleration induced by both these parameters is larger and comparable during September–December.

## 1. Introduction

Low-latitude mesospheric winds are characterized by semiannual oscillation (MSAO) with westward maxima during equinox months and eastward or less westward winds during solstice months (Andrews et al., 1987; Garcia et al., 1997; Reed, 1966). This oscillation is approximately 3 months out of phase with the stratospheric semiannual oscillation (SSAO). It is known that the SSAO is mainly driven by advection of westward momentum by mean meridional circulation (Holton & Wehrbein, 1980) and momentum deposition due to vertically propagating waves of all scales, in particular Kelvin waves and inertia gravity waves contributing to its eastward phase. However, the driving mechanisms for the upper mesospheric semiannual oscillation are not well understood. Considering the out-of-phase relationship between SSAO and MSAO (Antonita et al., 2007), Dunkerton (1982) suggested that the selective transmission of Kelvin waves and gravity waves by SSAO could drive the MSAO. Sassi and Garcia (1997) suggested the possible role of inertia-gravity waves of convective origin that

© 2026. American Geophysical Union. All Rights Reserved.

could drive the westward phase of the MSAO and both inertia-gravity waves and Kelvin waves contributing to the eastward phase.

There is an equinoctial asymmetry exhibited sometimes by the MSAO with a westward wind maximum during March-April being stronger than September-October and the large westward winds occur preferentially during the eastward phase of stratospheric quasi-biennial oscillation (QBO) (Burrage et al., 1996; Garcia et al., 1997). The large westward winds were suggested to be due to selective filtering of inertia gravity waves (Sassi & Garcia, 1997) and/or small-scale gravity waves generated due to tropical convection (Beres et al., 2005; Dunkerton, 1982). Using the equatorial beta-plane model, Garcia and Sassi (1999) demonstrated that the inertial gravity waves of phase speeds slower than 40 m/s, which are important for driving the westward phase of MSAO, could get absorbed by the strong westward phase of the QBO, while they can propagate to mesospheric heights during their eastward phase without any attenuation. As the eastward phase of QBO winds is weak (∼15 m/s), similar quasi-biennial modulation of MSAO could not occur during the eastward phase of QBO.

Using the Whole Atmosphere Community Climate Model, version 2 (WACCM2), Richter and Garcia (2006) demonstrated that the meridional advection of the zonal wind (∼−9 m/s/day) and Eliassen-Palm flux divergence from resolved waves (∼−8 m/s/day mostly due to quasi-2-day wave) could also contribute significantly to the momentum budget of the MSAO and they counter the eastward forcing due to small-scale gravity waves. Their results also suggested that small scale gravity waves could not be the primary driver of the MSAO near the equinoxes and the westward forcing must be due to inertia-gravity waves and tides, which have been accurately represented in WACCM2.

Akmaev et al. (1996) suggested that convective instabilities may lead to the damping of migrating diurnal tides. Lieberman and Hays (1994) quantitatively estimated that the contribution due to diurnal tide to the westward phase to be up to −20 m/s/day near the equinoxes at 100 km, and less than −5 m/s/day near 85 km. Sridharan (2020) observed that the migrating diurnal tide (DW1) estimated from Sounding of Atmosphere by Broadband Emission Radiometry (SABER) temperature at 80–90 km shows larger amplitudes in March than in September in 2008 and 2011, which seems to be consistent with the large equatorial mesospheric mean westward winds in March than in September in these strong La Niña years. The results also showed that the DW1 was equinoctially symmetric during the equatorial mesospheric mean zonal wind exhibiting equinoctial symmetry.

The induced westward acceleration could drive poleward residual flows and transport angular momentum poleward from the equator (Holton & Wehrbein, 1980). The extension of residual flows from one hemisphere to the opposite hemisphere could cause a more pronounced acceleration of westward winds at the equator (Tomikawa et al., 2008). Using a newly developed reanalysis data sets, Suclupe et al. (2024) demonstrated the causes for the large westward wind (−80 m/s) observed at 82 km during March 2023 could be due to the large eastward winds at low levels, which blocked the eastward propagating waves. Garcia (2023) suggested that breaking of the diurnal tide could have a major impact on the zonal wind structure in the mesosphere and lower thermosphere during the equinoxes.

Though it is not yet clear what governs the westward flows at the upper mesosphere and lower thermosphere (UMLT) heights and their interannual variability, there has recently been a consensus among the scientific community on the potential role of the migrating diurnal tide in driving the large westward winds in the upper mesospheric heights. In the present work, we investigate seasonal and interannual variabilities of upper mesospheric semiannual oscillation and their possible link with the tidal forcing using space-borne horizontal wind observations.

## 2. Data and Methodology

### 2.1. Horizontal Winds From ICON/MIGHTI

On 10 October 2019, NASA launched the Ionospheric Connection Explorer (ICON) satellite into a nearly circular orbit at an altitude of ∼575 km with an inclination of 27° (Englert et al., 2023; Li et al., 2024). Michelson Interferometer for Global High Resolution Thermospheric Imaging (MIGHTI) is one of the four instruments onboard ICON and it measures horizontal thermospheric winds in the altitude region 90–300 km covering latitudes from 12°S to 42°N. Two perpendicularly oriented interferometers MIGHTI-A and MIGHTI-B making an azimuth angle of 45° and 135°, respectively, from the spacecraft ram direction use the Doppler Asymmetric Spatial Heterodyne Spectroscopy (DASH) technique to estimate the line of sight (LOS) winds based on the Doppler shift

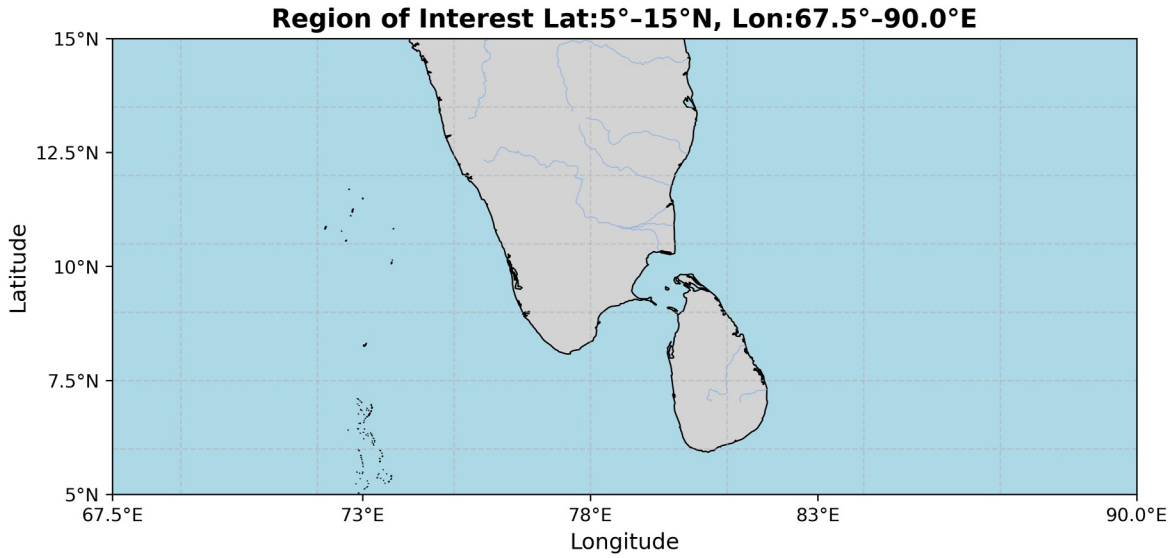


**Figure 1.** Geographical map of the region of interest for the present study having latitude and longitude range as 5°N–15°N and 67.5°E–90°E.

measurements of the forbidden atomic oxygen red and green lines from airglow emissions centered at wavelengths 630.0 nm (O ($^1$D → $^3$P)) and 557.7 nm (O ($^1$S → $^1$D)). Dissociative recombination and the collisional deactivation of $N_2$ are the main airglow production processes, respectively (Gao et al., 2024). Thus, the LOS wind velocities obtained from the two sensors (MIGHTI-A and MIGHTI-B), after coordinate transformation, are combined to obtain the zonal and meridional winds.

Daytime data covers altitudes from 90 to 300 km for green-line winds and from 160 to 300 km for red-line winds, whereas nighttime data are available from 90 to 110 km and 220–300 km and with vertical resolution of ∼3 and ∼10 km for green-line and red-line winds, respectively (Meenakshi & Sridharan, 2024). It takes a complete precession period of about 48 days for ICON satellite passes to cover all the local times of 0–24 hr over a region (Englert et al., 2023). In the present work, the Version 5 (vr5) Level 2.2 data products are used. The quality of the available data was classified as 0.0 (Bad), 0.5 (Caution), 1.0 (Good) and we have selected only those data for which the variable "ICON_L22_Wind_Quality" = 1.0.

### 2.2. Tidal Analysis From MIGHTI Zonal and Meridional Winds

In our present study, we used version 5 Level 2.2 green-line vector wind data from 6 December 2019 to 24 November 2022. The region of interest has a latitudinal extent of 5°N–15°N and longitudinal extent of 67.5° E–90.0°E (Figure 1). To obtain full local time coverage over this region, we have restricted the altitude range from 91 to 109 km with a vertical resolution of 3 km. The wind values for about 2 months are binned for each 1 hr to obtain the diurnal cycle of winds from 1 to 24 hr. For example, to obtain complete local time coverage for 1 January 2020, we have binned data from 6th December 2019 to 31st January 2020. Following this, we have obtained monthly profiles of zonal and meridional winds from January to December for 2020, 2021 and from January to November in 2022 (since the last valid data is available till 24 November 2022).

Now for the extraction of tidal amplitudes, the zonal and meridional winds obtained are interpolated to have 1-hr temporal resolution for each month to obtain *u(t)* and *v(t)*, which are subjected to a classical harmonic analysis via the following equation

$$u(t), v(t) = a_0 + \sum_{n=1}^{n=3}\left(C_n \sin\left(\frac{2\pi}{T_n}t + \phi_n\right)\right) \quad (1)$$

where, $a_0$ is the mean wind, $C_n$ and $\phi_n$ are the amplitude and phase of the $n$th tidal components with $n = 1, 2, 3$ corresponding to 24-hr (diurnal), 12-hr (semi-diurnal) and 8-hr (ter-diurnal) tides (Dutta & Sridharan, 2023). The harmonic fit is independently applied to *u(t)* and *v(t)* using the least squares method. Here, $C_n$ denotes the

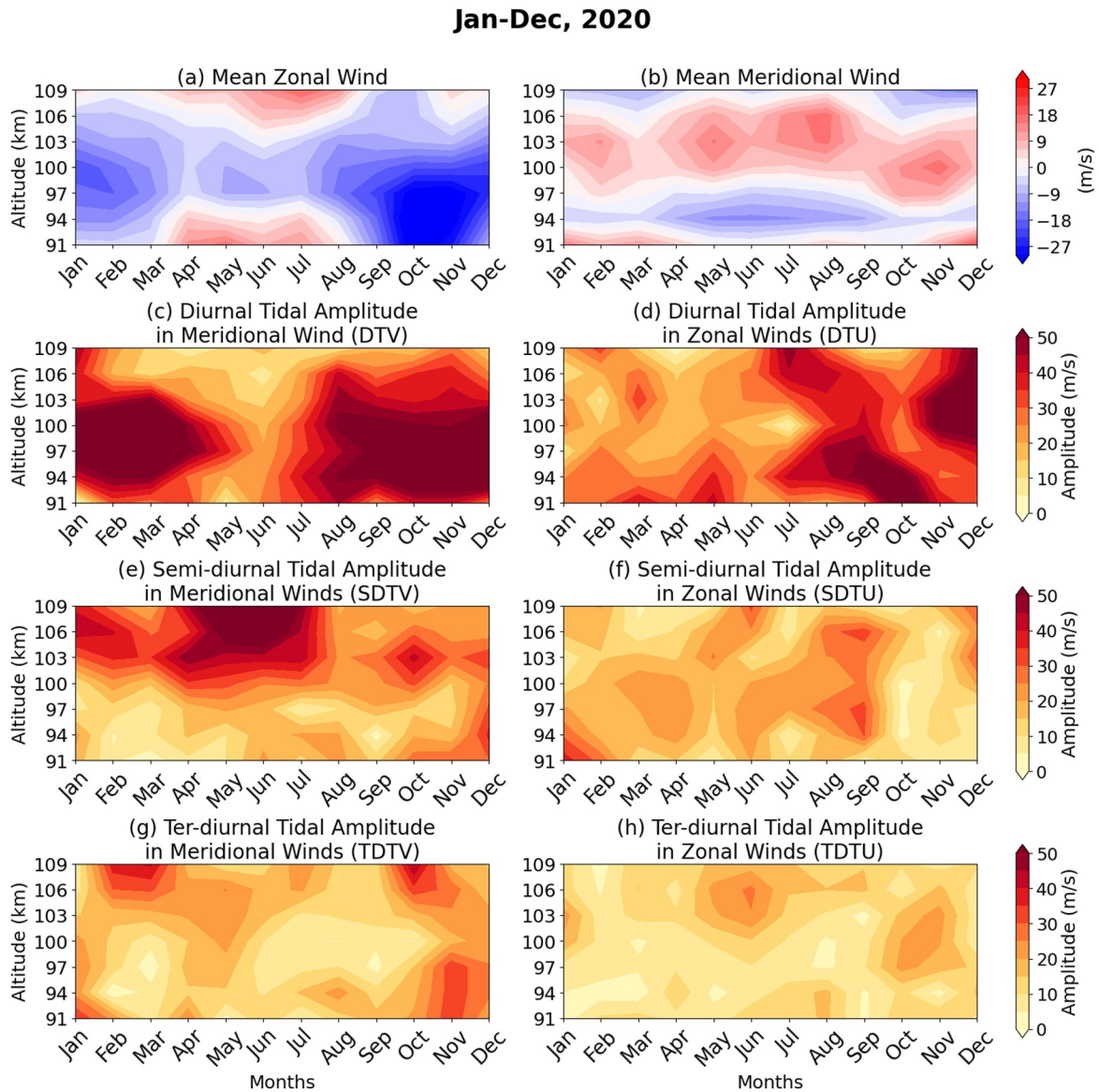


**Figure 2.** Seasonal variation of (a) mean zonal wind, (b) mean meridional wind, (c) diurnal tidal amplitude in meridional wind (DTV), (d) diurnal tidal amplitude in zonal wind (DTU), (e) semi-diurnal tidal amplitude in meridional wind (SDTV), (f) semi-diurnal tidal amplitude in zonal wind (SDTU), (g) ter-diurnal tidal amplitude in meridional wind (TDTV) and (h) ter-diurnal tidal amplitude in zonal wind (TDTU) for the year 2020 for the altitude range 91–109 km.

amplitudes for diurnal (DTU), semi-diurnal (SDTU) and ter-diurnal (TDTU) tides in zonal wind as well as for diurnal (DTV), semi-diurnal (SDTV) and ter-diurnal (TDTV) tides in meridional wind, obtained by fitting $u(t)$ and $v(t)$ in Equation 1. The analysis is repeated successively for every month to obtain seasonal variation of the tidal amplitudes for the years 2020–2022.

## 3. Results

Figures 2a–2h, 3a–3h, and 4a–4h show the variation of monthly mean zonal winds (m/s) and meridional Winds (m/s) along with monthly diurnal, semi-diurnal, and ter-diurnal amplitude (m/s) of both Zonal and Meridional winds from ICON/MIGHTI (91–109 km) green-line v5 winds for the years 2020, 2021, and 2022, respectively. The latitudinal and longitudinal extents for the study were taken to be 5°N–15°N and 67.5°E–90.0°E, respectively.

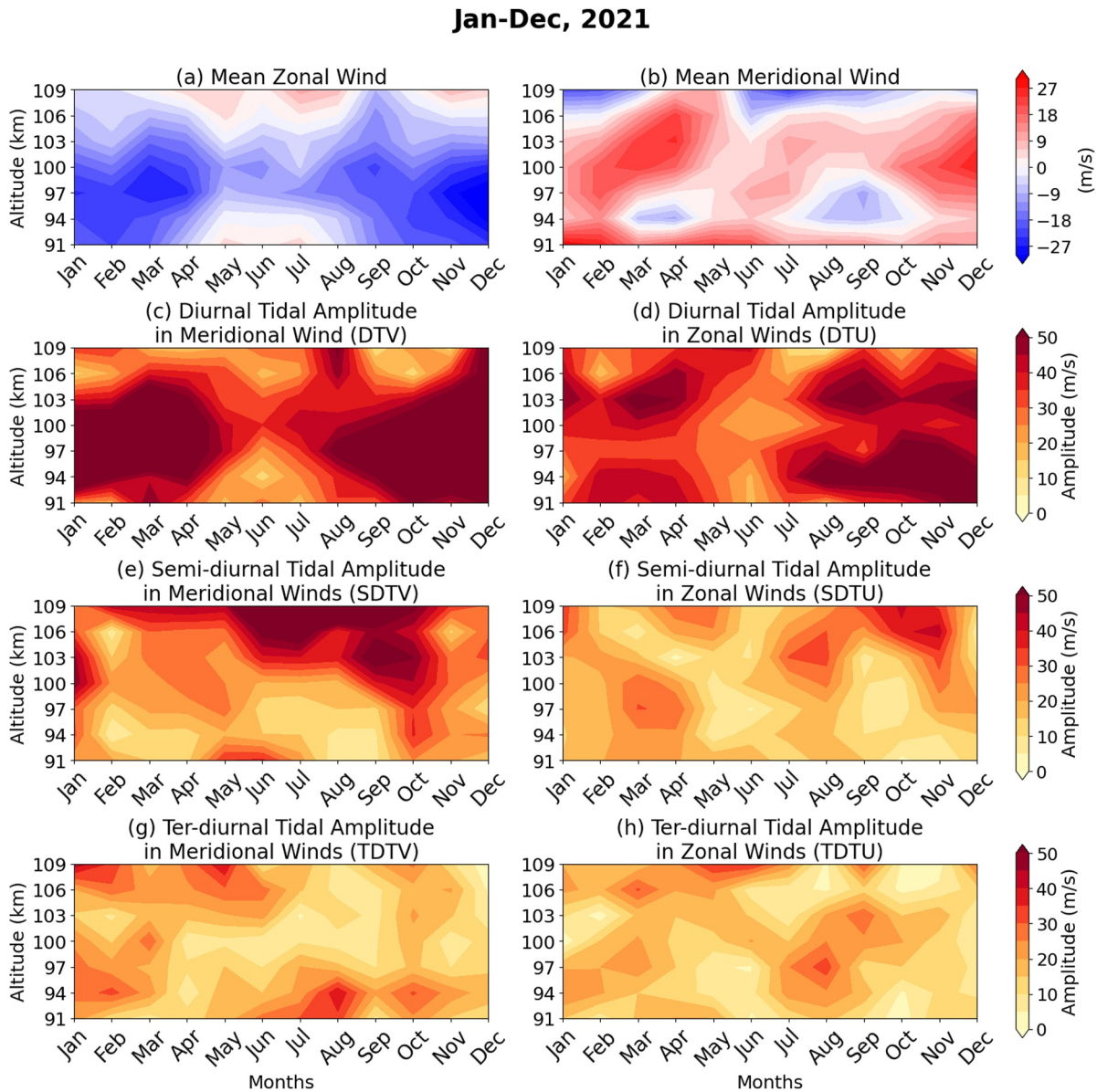


**Figure 3.** Same as Figure 2 but for the year 2021.

### 3.1. Seasonal Variation of Mean Winds and Tidal Amplitudes in 2020

Figures 2a–2h shows the monthly variation of mean zonal and meridional winds (in m/s) along with the Diurnal ($n = 1$), Semi-diurnal ($n = 2$), and finally Ter-diurnal ($n = 3$) tidal amplitude in zonal wind (DTU, SDTU, TDTU), and Meridional wind (DTV, SDTV, TDTV) for the year 2020. Figure 2a shows the seasonal variation of mean zonal winds (m/s). During the months of January-March we see a gradual intensification of westward winds from ∼−3 m/s at 91 km altitude to −20 m/s near 100 km, followed by gradual weakening of westward winds above 100 km until we find mild eastward winds (∼2 m/s) at 109 km. Similarly, from September to December, we find strong westward winds prevailing from 91 to 97 km peaking around October (∼−40 m/s) at 94 km. Thereafter, above 100 km, a subsequent decrease in westward winds followed by weak eastward winds around 109 km can be seen.

From Figure 2c, from January to April, we see that at lower heights (∼91 km) diurnal tidal amplitude in meridional wind (DTV) shows a minimum in January and it increases to ∼30 m/s during February-April. As we approach higher altitudes, DTV increases and reaches a maximum (∼80 m/s) around 100 km altitude in March.

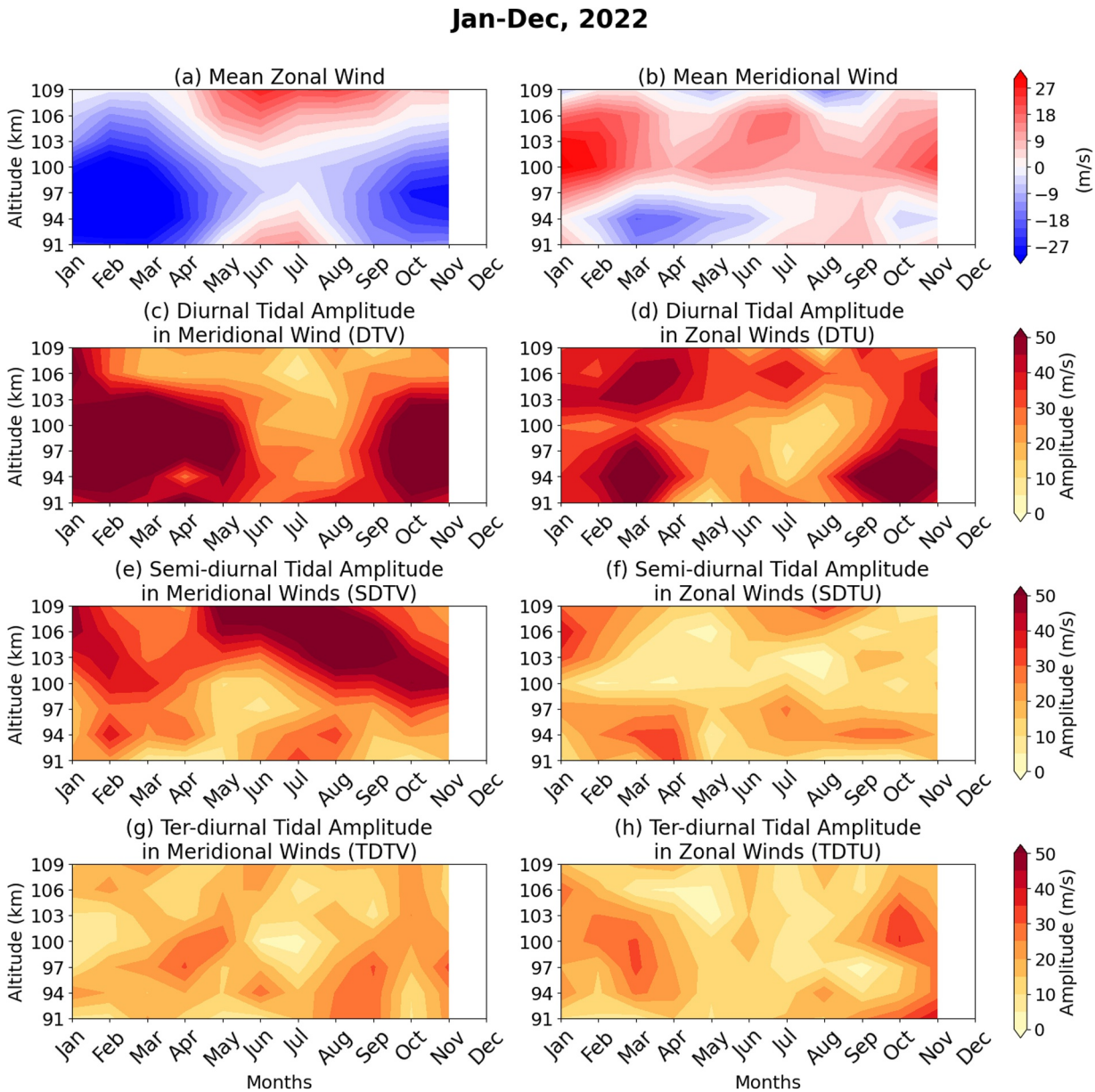


**Figure 4.** Same as Figure 2 but for the year 2022.

From 103 to 109 km, we see the strength of DTV again decreases, thus showing its strongest signatures from 94 to 100 km during February-April. Similarly, during the months of August-December, DTV begins to increase from ∼40 m/s around 91 km, reaches its peak of ∼75 m/s at 97 km in December and deceases above 97 km, showing the weakest amplitude signal (∼17 m/s) in December at 109 km. Thus, seasonal variation of DTV exhibits a striking similarity with the subsequent strengthening and weakening of mean westward winds for the same months and over the same altitude range. Hence, it can be expected that the diurnal tide in meridional wind may have transferred its westward momentum into the background zonal flow due to tidal damping.

DTV ceases over the months of May–July lacking a clear seasonal amplification as seen during January–April and August–December. Similarly, from May to July we see a transition of eastward to westward winds (Figure 2a) from 91 to 100 km followed by a shift in wind direction above 100 km. At higher altitudes (>103 km) in Figure 2e, a strong semi-diurnal component in Meridional wind (m/s) (SDTV) persists from May to July with its peak (80 m/s) in June at 109 km. The seasonal amplification pattern in SDTV shows a close resemblance with mean eastward

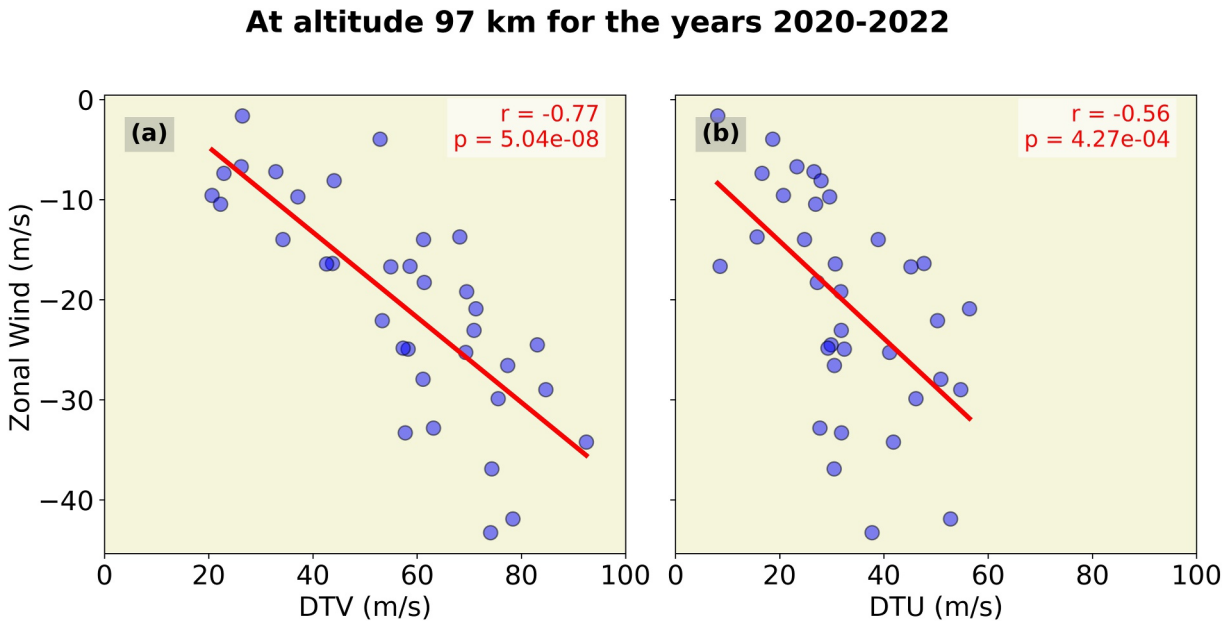


**Figure 5.** Scatter plot of zonal wind (m/s) versus (a) DTV (m/s) and (b) DTU (m/s) at 97 km for the years 2020–2022.

winds at higher altitudes. Unlike DTV, diurnal tidal amplitude in zonal wind (DTU) in Figure 2d does not show any such seasonal and altitudinal resemblance with the westward wind intensification. Since DTU has almost similar magnitude (m/s) to DTV from 91 to 94 km from August to October, it can be thought to strengthen the westward flow. SDTU, TDTV, and TDTU (Figures 2f–2h) exhibit weaker magnitude (m/s) with no clear seasonal variation. For the year 2020, we see a shift from poleward (∼15 m/s) to equatorward winds peaking in May-July (∼−12 m/s) from 91 to 94 km, as depicted by Figure 2b. Above 97 km, poleward winds persist across all seasons peaking in August at 106 km and thereafter become sufficiently equatorward with maximum intensity over February–March (−10 m/s) and November–December (−14 m/s) around 109 km.

### 3.2. Seasonal Variation of Mean Winds and Tidal Amplitudes in 2021

Figure 3a shows the seasonal variation of mean zonal winds (m/s) for the year 2021. During January–April we see westward winds prevailing from 91 km and reaching its peak (∼−23 m/s) around 97 km in the month of March followed by a gradual weakening above 100 km. Similarly, from September to December, strong westward winds are found at 97 km (∼−35 m/s) peaking around December followed by a gradual shift of westward to weak eastward winds (∼2 m/s) at 109 km during October-December. DTV also shows an almost similar seasonal variation in its magnitude (Figure 3c) having the lowest value (∼20 m/s) at 91 km in February and attaining its highest peak (∼100 m/s) in March around 100 km followed by further damping to 18 m/s in January at 109 km. Similar to the height structure of amplitude in January-March, the DTV during September-November is minimum (∼32 m/s) in September around 91 km and maximum of (∼96 m/s) at 97 km in December.

Very weak eastward winds (∼2 m/s) can be observed at 91 km during May-July followed by wind reversal from 94 to 103 km. Figure 3e at 109 km, presence of large SDTV attaining a peak value (∼95 m/s) during July-August coinciding with weak eastward winds for the same. Diurnal tidal amplitude in zonal wind (DTU) has magnitude comparable to DTV (Figure 3d) strictly from 91 to 94 km, which could result in the amplification of westward winds over this altitude above which DTV dominates, solely. As observed in 2020, the SDTU, TDTV, and TDTU do not show prominent seasonal enhancements (Figures 3f–3h).

A shift in meridional winds from poleward to equatorward wind can be seen from 91 to 94 km but only for the months March-April and August-October with wind velocity close to −10 m/s in the year 2021. Above 94 km, poleward winds sustain throughout the seasons till 106 km except around September (−10 m/s) at 97 km and June (∼−8 m/s) at 106 km. From 106 to 109 km, the development of strong equatorward winds from January to March (−20 m/s) and June to September (∼−22 m/s) can be seen in Figure 3b.

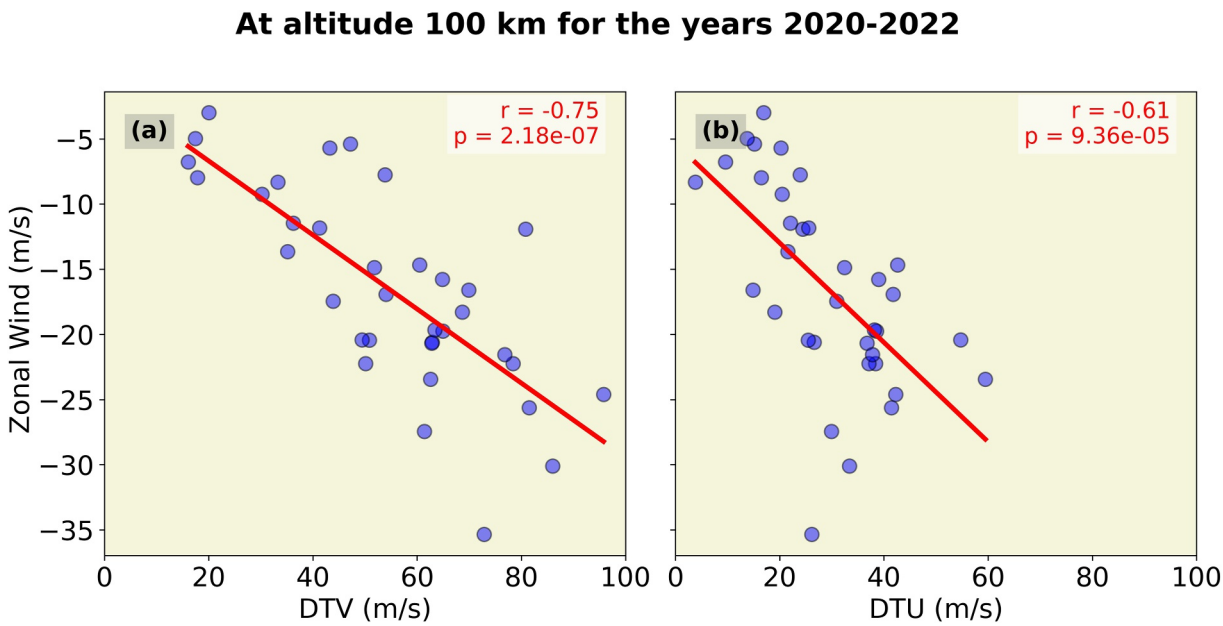


**Figure 6.** Scatter plot of zonal wind (m/s) versus (a) DTV (m/s) and (b) DTU (m/s) at 100 km for the years 2020–2022.

### 3.3. Seasonal Variation of Mean Winds and Tidal Amplitudes in 2022

Figure 4a shows the seasonal variation of mean zonal winds (m/s) for the year 2022. Sufficiently strong westward winds persist during January–April from 91 km and attain maximum intensity (∼−43 m/s) around 97 km from February to March followed by a gradual weakening above 100 km. During September–November, winds are relatively weak westward (∼−17 m/s) around 91 km and reach a maximum at 97 km (∼−24 m/s) in November. As altitude increases, a gradual change to weak eastward winds (∼15 m/s) is observed during September-November at 109 km. The seasonal variation of DTV in Figure 4c shows the lowest value (∼40 m/s) over January at 91 km, thereby attaining its highest peak (∼85 m/s) in March around 100 km, followed by further damping to 20 m/s in January at 109 km. Similar to the variation in January-April, DTV attains a dip (∼20 m/s) in August around 94 km and shows maximum amplitude (∼78 m/s) in November close to 100 km. Eastward winds (∼17 m/s) can be seen over the months of May–August at 91 km followed by wind reversal from 94 to 100 km. Eastward winds persist from 106 to 109 km during May–November having its peak (∼26 m/s) in June. SDTV starts dominating from 103 km and the highest value can be seen in June at 109 km. The variation in mean eastward winds shows almost symmetric behavior with the variation of SDTV at higher altitudes (>106 km).

Diurnal tidal amplitude in zonal wind (DTU) has magnitude comparable to DTV (Figure 4d) strictly from 91 to 94 km, which could result in amplification of westward winds over this altitude and above which DTV dominates, solely. Figures 4f–4h shows very weak seasonal variation and amplification of SDTU, TDTV, and TDTU, respectively. The scatter plots in Figures 5a and 6a are a vivid representation of how the amplification of DTV is strongly correlated with the intensification of westward winds. The negative sign in Pearson's correlation coefficient, $r = -0.77$ in Figure 5a and $r = -0.75$ in Figure 6a arises due to the negative sign in zonal wind, which affirms that with an increase in the magnitude of DTV (m/s), there is a similar strengthening of mean westward winds at 97 and 100 km altitude, respectively. From Figures 5b and 6b we can see diurnal tidal amplitude in zonal wind shows somewhat lesser correlation ($r = -0.56$ and $r = -0.61$, respectively) with westward intensification of mean winds compared to diurnal tidal amplitude in meridional wind. Nevertheless, the results are statistically significant owing to the p-value being much smaller than 0.05 for both zonal and meridional tidal components at 97 and 100 km altitude.

In 2022, unlike previous years, the equatorward winds strengthen from 91 to 94 km during February-June peaking around March (∼−19 m/s) along with poleward winds sustaining during July–September (∼8 m/s). Strong poleward winds, having maximum intensity (32 m/s) in January at 100 km can be seen to develop over all the

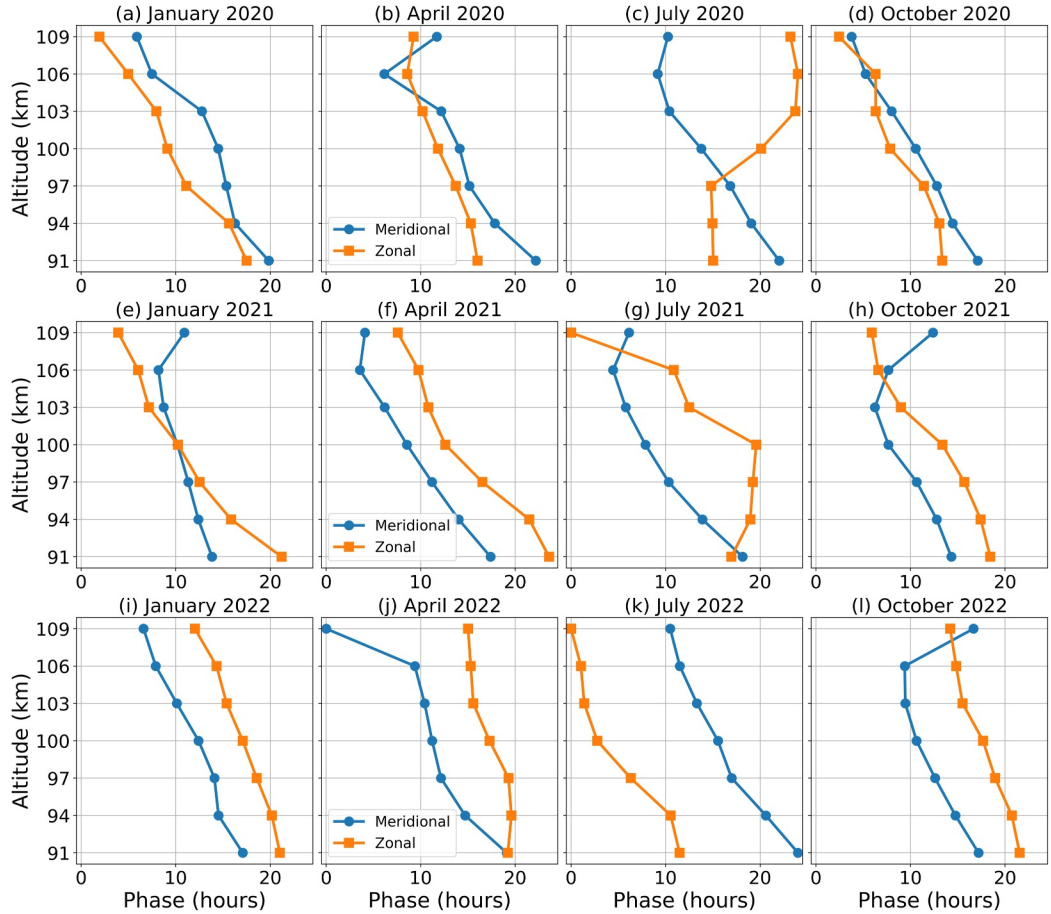


**Figure 7.** Seasonal phase profiles of diurnal tides January, April, July, and October for the years 2020 (a–d), 2021 (e–h) and 2022 (i–l).

months till 106 km and thereafter a shift to equatorward winds is noticed for the months of January, April–June, and August–September (−15 m/s) at 109 km in Figure 4b.

### 3.4. Seasonal Phase Profiles and Vertical Wavelengths

The phase profiles for diurnal tide in both zonal and meridional winds are shown in Figures 7a–7l. On average, meridional ($\phi_{\text{Meridional}}$) and zonal ($\phi_{\text{Zonal}}$) phases profiles for the 3 years show characteristic downward phase progression with time which indicates upward wave propagation with $\phi_{\text{Zonal}}$ showing somewhat irregular phase structures for few months such as in July 2020 (Figure 7c) and 2021 (Figure 7g)). The phase profiles for January show consistent phase progression for the years 2020 (Figure 7a), 2021 (Figure 7e) and 2022 (Figure 7i) in both $\phi_{\text{Meridional}}$ and $\phi_{\text{Zonal}}$ with the steepest rate of change of phase (∼3 km/hr) with height from 13 hr at 91 km to 9 hr at 103 km observed in 2021 in $\phi_{\text{Meridional}}$ as shown in Figure 7e. We see a similar sharp gradient in $\phi_{\text{Zonal}}$ (∼4 km/hr) from 19 hr at 91 km to 15 hr at 109 km in April 2022 (Figure 7j). Beyond 103 km, few months like October 2021 (Figure 7h), 2022 (Figure 7l) and April 2020 (Figure 7b), we see increasing phase shift with height in $\phi_{\text{Meridional}}$.

Figures 8a–8c represents the vertical wavelengths ($\lambda_Z$) of diurnal tides in zonal and meridional winds are calculated from their phase variation with height. It is observed that the wavelength of the meridional tide ($\lambda_{\text{Meridional}}$) is in the range of 25–30 km during January–March, and during September-December but relatively shorter (∼18 km) during May-July in 2020 (Figure 8a). Though similar seasonal variation of vertical wavelength is observed in both 2021 and 2022, $\lambda_{\text{Meridional}}$ is much longer (∼58 km) in January 2021. The vertical wavelength of zonal tide ($\lambda_{\text{Zonal}}$) has a maximum wavelength during the months of May (40 km) and September (38 km) in 2020, June (46 km) and September (40 km) in 2021 and April (48 km) in 2022 where, $\lambda_{\text{Zonal}}$ is higher than $\lambda_{\text{Meridional}}$. Considerably longer $\lambda_{\text{Zonal}}$ (30–40 km) can be seen from January to March in 2021 and 2022 than in

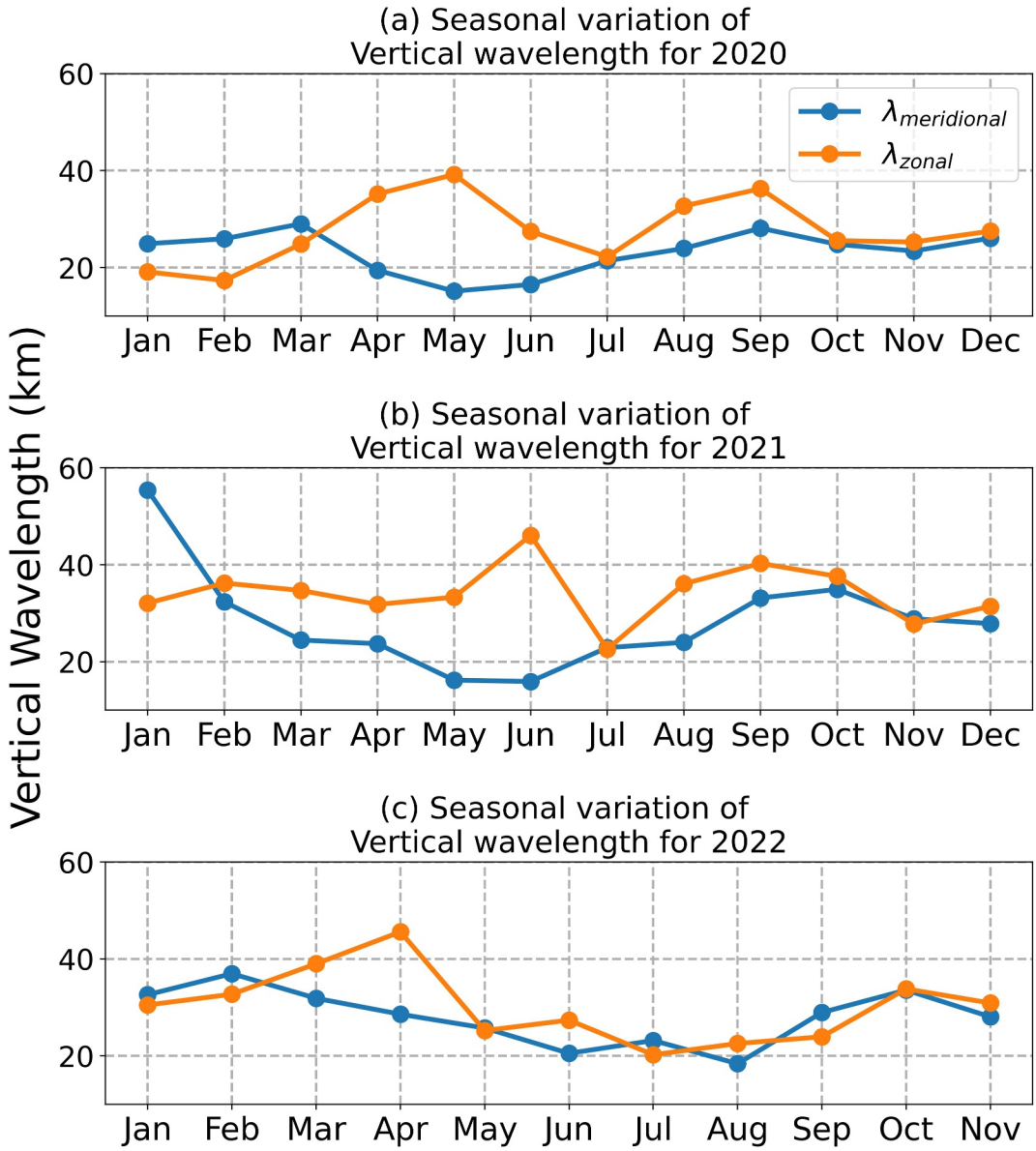


**Figure 8.** Seasonal variation of vertical wavelength (km) of diurnal tide for the years (a) 2020, (b) 2021 and (c) 2022.

2020 (~20 km). In all three years, minimum $\lambda_{\text{Zonal}}$ (~20 km) is found during the month of July. Sharp gradient in phase progression with height indicates large vertical wavelengths (Figures 8b and 8c) and the results are in coherence with the phase profiles of January 2021 and April 2022, as shown in Figures 7e and 7j, respectively.

### 3.5. Mean Zonal Flow Acceleration From Momentum Fluxes

The acceleration of the mean zonal wind due to tidal wave dissipation can be estimated as

$$\frac{d\overline{U}}{dt} = -\frac{1}{\rho_0}\frac{\partial}{\partial z}(\rho < u'w' >) \tag{2}$$

where, $\overline{U}$ is the mean zonal wind, $\rho_0$ is mean density, $< u'w' >$ is the time-averaged zonal and vertical diurnal tidal velocity terms, respectively. The divergence of the vertical flux of zonal momentum $(\frac{1}{\rho_0}\frac{\partial}{\partial z}(< \rho u'w' >))$, can be estimated using the polarization relation $w' = -\frac{k}{m}u'$, where $k$ and $m$ are the horizontal and vertical

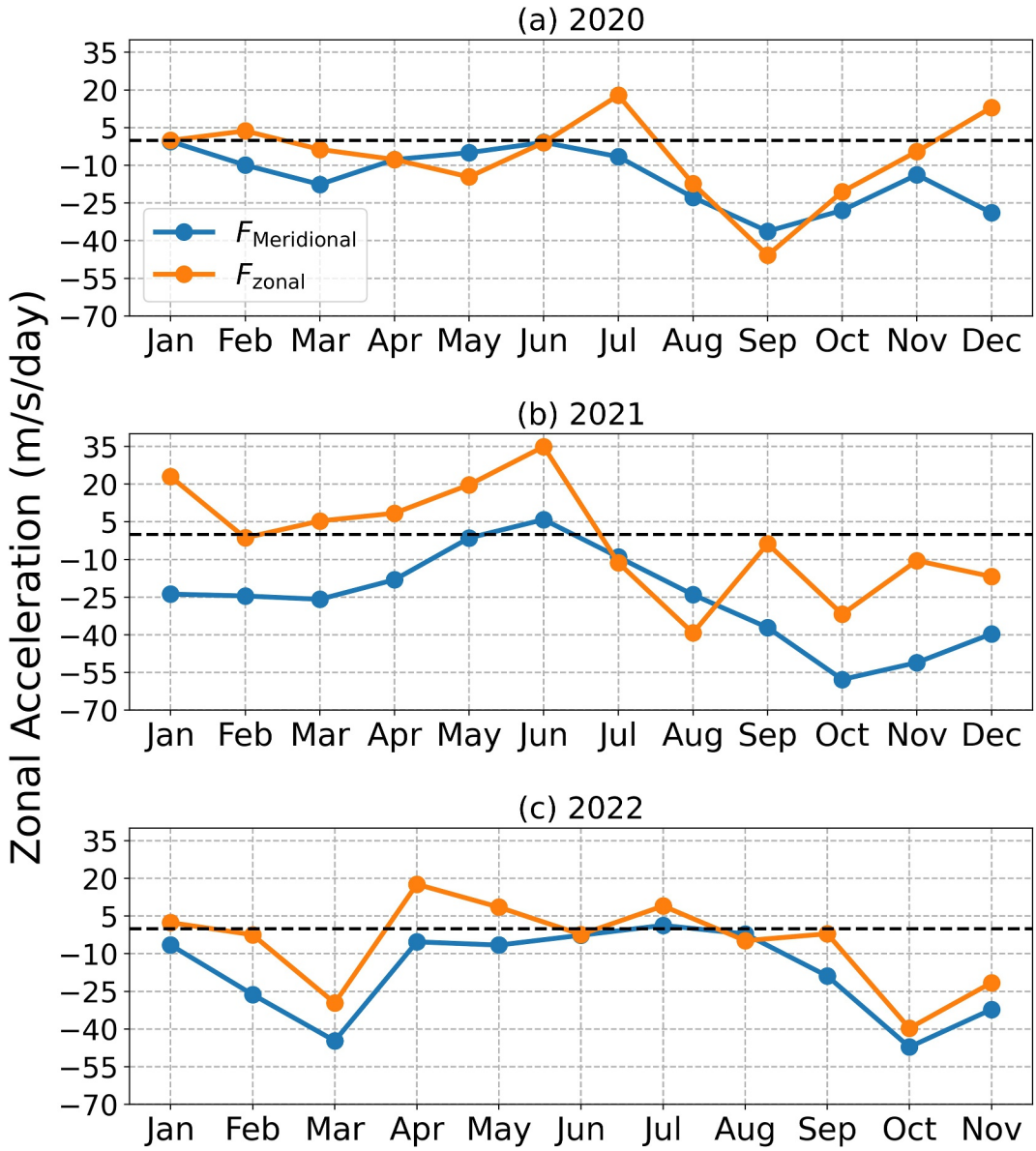


**Figure 9.** Seasonal variation of zonal acceleration (m/s/day) for the years (a) 2020, (b) 2021 and (c) 2022. In this Figure, the black dashed line (--) indicates zero zonal acceleration.

wavenumbers, respectively. As we have observed, DTV has a strong vertical and seasonal correlation with simultaneous strengthening/weakening of westward winds in all 3 years, and the westward momentum induced by the convergence of meridional flux is also considered. As the diurnal tide in meridional wind shows similar seasonal variation as that of migrating diurnal tide (DW1) and also the amplitude of non-migrating tides is in general much less when compared to that of DW1 (Sridharan, 2019), it is assumed that the diurnal tide mostly represents the DW1 and horizontal wavelength of DW1 is used here in the calculation of zonal acceleration. The height variation of atmospheric density has been obtained from the NRLMSIS version 2.0 atmospheric model (Emmert et al., 2021).

Figures 9a–9c gives us the seasonal variation of zonal acceleration (m/s/day) at 97 km induced by the horizontal momentum flux divergence $F_{\text{zonal}}$ and $F_{\text{meridional}}$ given as

$$F_{\text{zonal}} = -\frac{k}{m\rho_0}\frac{\partial}{\partial z}(\rho < u'^2 > ) \tag{3}$$

$$F_{\text{meridional}} = -\frac{k}{m\rho_0}\frac{\partial}{\partial z}(\rho < u'v' >) \quad (4)$$

where in Figure 9a, $F_{\text{meridional}}$ and $F_{\text{zonal}}$ induce westward acceleration close to −18 m/s/day and −14 m/s/day in the month of March and May, respectively. The westward acceleration is found to be very low during the months of April–July. However, $F_{\text{zonal}}$ shows eastward acceleration (∼20 m/s/day) in the month of July. From August to November, both $F_{\text{zonal}}$ and $F_{\text{meridional}}$ impart large westward acceleration peaking around the month of September (∼−40 m/s/day), which is in accordance with the large mean westward winds (Figure 2a) found during these months in 2020. The convergence of the meridional momentum flux is found to be consistent throughout January to March, causing westward acceleration of −25 m/s/day and thereby gradually diminishing in strength until July 2021, as shown in Figure 9b. The westward acceleration due to $F_{\text{meridional}}$ gradually increases from August to November reaching its maximum in October (−55 m/s/day). Unlike $F_{\text{meridional}}$, the divergence in $F_{\text{zonal}}$ causes an eastward acceleration from January to a maximum of 35 m/s/day in the month of June. The zonal acceleration induced by $F_{\text{zonal}}$ reverses its direction from July to December, where the strength of westward acceleration varies alternatively within −40 m/s/day and −2 m/s/day. The strength of the westward acceleration induced by convergence of meridional momentum flux ($F_{\text{meridional}}$) shows excellent correlation with the seasonal variation of mean westward winds at 97 km (Figure 3a), suggesting the driving of the zonal mean flow due to tidal momentum dissipation. Unlike 2020 and 2021, Figure 9c shows a symmetric enlargement of westward acceleration induced by both $F_{\text{meridional}}$ and $F_{\text{zonal}}$ from January to a maximum in March (∼−43 m/s/day) and from September to a maximum in October (∼−47 m/s/day) which shows a similar seasonal variation with the large mean westward winds as shown in Figure 4a in 2022. Tidal dissipation due to convergence of meridional flux is found to be very weakly westward (∼−5 m/s/day), which appears to be consistent with weak mean westward winds prevailing from April to August.

## 4. Discussion

In the present study, the ICON/MIGHTI zonal and meridional winds are utilized to study seasonal variation of mean zonal and meridional winds and diurnal, semi-diurnal and ter-diurnal tides from 91 to 109 km with the region of interest having a latitudinal and longitudinal extent of 5°N–15°N and 67.5°E–90°E, respectively, for the years 2020, 2021, and 2022. Semiannual variation of mean westward winds is noticeable in all the three years between 91 and 106 km. Large westward winds are found to dominate around 97–100 km from September to November in 2020 and 2021 and from January to March in 2022. Studies from Yamazaki et al. (2023) show ICON/MIGHTI zonal-mean zonal wind to be weakly westward below ∼105 km within the equatorial region (10°S–10°N). The reversal of zonal-mean zonal wind is often seen around 105 km, which has been confirmed by Yiğit et al. (2022). Consistent with our present study, Lieberman and Hays (1994) observed the presence of mean easterly flow at 90–105 km with a similar semiannual variation in the space-borne High Resolution Doppler Imager (HRDI) wind observations. Lieberman et al. (1993) and Garcia et al. (1997) also reported the presence of semiannual oscillation of mean easterly flow above 65 km with maximum intensity occurring near equinox periods. The amplitude of migrating diurnal tidal amplitude in meridional wind in Yamazaki et al. (2023) is found to be largest at 15°N–20°N around 95–97 km and shows a distinct semiannual variation with equinoctial maxima of ∼60 m/s. Similarly, studies like Meenakshi & Sridharan, 2024 and Teja et al. (2024) used ICON/MIGHTI winds over low latitude regions and reported a distinct semiannual oscillation of migrating diurnal tide in meridional wind with maximum amplitude (∼65–100 m/s) around equinoxes and minimum amplitude (<40 m/s) during solstices from 94 to 100 km. In the present study, it was found that the diurnal tidal amplitude in meridional wind (DTV) shows strikingly similar seasonal amplification with the semiannual variation in westward winds in the altitude region 91–103 km. In all the three years, a semiannual maximum in diurnal tidal amplitude in meridional wind can be seen in March (80 m/s–100 m/s) and from November to December (75 m/s–96 m/s), followed by a minimum from May to July (∼20 m/s) at 97–100 km altitude. Thus, this semiannual oscillation reported in our study seems to be highly concurrent with earlier ICON/MIGHTI low latitude studies. Consistent with our results, Zhang et al. (2007) reported the presence of larger meridional diurnal tidal amplitude in the winds observed by the space-borne Wind Imaging Interferometer (WINDII) instrument. They also reported that the equinoctial amplitudes are 2–4 times that of the solstitial minima, as observed in the present study. Using SKiYMET radar observations at Trivandrum (8°N, 77°E), Deepa et al. (2006) confirmed the diurnal tide in meridional wind to be stronger than the zonal wind. The dominant source of excitation of migrating semi-diurnal

tides in MLT altitudes is heating resulting from the absorption of UV radiation by ozone peaking around 45 km (Forbes & Garrett, 1978; Forbes et al., 2022). In our study, we see a strong semi-diurnal component in meridional wind (80–90 m/s) that persists from May to August above 103 km. Similarly, using ICON/MIGHTI green-line measurements, Yamazaki et al. (2023) and Meenakshi & Sridharan, 2024 also found the amplitude of migrating semi-diurnal tides reaching 60 m/s above 100 km during August-September and March-September, respectively. Miyahara (1981) earlier reported a large westward wind (−40 m/s) in the low latitude region at an altitude of 100 km and indicated that the dissipating solar diurnal tidal wave could contribute to the determination of the mean zonal wind structure in the lower thermosphere. Hagan (1999) observed a similar semiannual variation in diurnal tidal amplitude in the meridional winds observed by the HRDI instrument around 20°N with maximum amplitude in March and October (∼60–70 m/s) at 95 km.

Based on the availability of both satellite and radar observations, we methodically selected our region of interest covering the radar sites in order to validate our results efficiently. Teitelbaum and Vial (1981) reported a distinct westward wind maximum at 10°N in March around 100 km and attributed it to the mechanical dissipation of the first propagating diurnal tide, which could induce an eastward acceleration beyond 20° latitude and westward from the equator and 20° latitude. In 2020 and 2021, we observe more intense westward winds from October to December compared to March at 97 km, whereas in 2022, maximum ICON/MIGHTI mean westward winds are captured during the month of March. Delisi and Dunkerton (1988) and Garcia et al. (1997) reported seasonal asymmetry in westward winds with stronger westward winds in the March equinox, when compared to September equinox. However, the present study reports that the westward winds in the fall equinox can also be stronger than the March equinox. It is also interesting to note that in those years, the diurnal tidal amplitude is also stronger in September equinox when compared to March equinox. Earlier, the interannual variability of the zonal wind was attributed to the eastward phase of the stratospheric quasi-biennial oscillation using upper mesospheric wind data for limited periods (Burrage et al., 1996; Rajaram & Gurubaran, 1998). However, Sridharan et al. (2007) with long-term mesospheric winds observed by the medium frequency radar at Tirunelveli (8.7°N, 77.8°E) confirm that large westward winds did not occur in all eastward phases of stratospheric QBO. In the present study, the vertical wavelength of the diurnal tide is found to be in the range from 18 to 40 km, with a rare occurrence of 58 km in January 2021. In earlier studies, the vertical wavelength of diurnal tide was found to be ∼25 km in Deepa et al. (2006) and ∼30 km in Roble and Ridley (1994) along with a downward propagating phase, both of which corroborate well with our results. In an isothermal atmosphere of 256 K, the migrating diurnal tide can have a vertical wavelength of 28 km, though it can be very significant in the real atmosphere (Chapman & Lindzen, 1970).

The upper mesosphere lower thermosphere (UMLT) region covering ∼50–180 km is dominated by wave dissipating processes governing the atmospheric dynamics and energetics. Vertically propagating planetary waves, with period range ∼2–25 days, transfer momentum into the middle atmosphere and play a significant role in UMLT dynamics. Using daily mean wind velocities obtained from MF radar over the low latitude region (16.8°N, 74.2°E) for four years (August 2013–July 2017), Gaikwad et al. (2023) observed a strong semiannual oscillation in 6.5-day wave with an equinoctial maximum, which appears to be stronger when the mean background winds are predominantly westward. Suresh Babu et al. (2012) calculated the forcing towards the mean flow by the 2–4 days and 6–8 days planetary waves in the 82–98 km height region using the horizontal and vertical winds obtained from SKiYMET Meteor Wind radar over Trivandrum (8.5°N, 77°E) and reported 30%–80% contribution from both 6–8 days and 2–4 days waves dominating during winter and vernal equinoxes and during summer and both equinoxes, respectively, during the period April 2006–April 2007. Besides planetary waves, comprehensive work has already been done to estimate the role of gravity waves in driving the MSAO over multiple latitude sites. Dunkerton (1982) suggested that the selective transmission of vertically propagating gravity waves of easterly and westerly phase speeds leads to a semiannually varying deposition of momentum in the mesopause region and can act as a plausible mechanism for the MSAO. The parameterization for the momentum deposition of small-scale gravity waves in the background flow developed by Hines (1997) was used extensively by Mengel et al. (1995) in Numerical Spectral Model (NSM) over low latitudes, which revealed that gravity wave interaction with mean zonal wind produces significant semiannual oscillation signatures in the zonal circulation of the upper mesosphere. Hitchman et al. (1992) found the mean flow forcing to be ∼10–100 m/s/day due to momentum fluxes by short period gravity waves from 70 to 85 km altitude using data from the MST radar at Jicamarca, Peru (12°S, 77°W) during two 10-day campaigns in June and August of 1987. Eswaraiah et al. (2013) estimated zonal (∼4 $m^2s^{-2}$) and meridional (∼10–12 $m^2s^{-2}$) momentum fluxes of gravity waves with

periods 20 min to 2 hr between 73 and 80 km using long-term observational data (1998–2008) from the MST Radar and Rayleigh LIDAR over a tropical station, Gadanki (13.5°N, 79.2°E). However, in both cases, the mean flow forcing and the momentum fluxes, respectively, seemed to oppose the mean background wind and were unable to conclude the role of gravity waves in driving the MSAO. From the calculated profiles of mean zonal acceleration from gravity wave momentum flux data using a dual-beam Doppler radar near Adelaide, Australia (35°S, 138°E) from 9 to 17 June 1984, Fritts and Vincent (1987) concluded a clear tendency towards convergence of easterly momentum between 80 and 96 km range leading to an easterly acceleration of the zonal mean flow. Almost 70% of this inferred zonal drag (−8 to −50 m/s/day) was contributed by high-frequency ($T < 1$ hr) gravity waves (Reid and Vincent (1987); Vincent and Reid (1983)). Observing wind variability at mesospheric altitudes, Nakamura et al. (1993) observed wind motions from 60 to 90 km altitude using MU Radar located at a midlatitude (35°N, 136°E) station and provided a quantitative value of gravity wave (period from 5 min to 8–10 hr) induced zonal and meridional drag to be +51 m/s/day and −4 m/s/day in June at 75 km and −4 m/s/day and +7.4 m/s/day in October at 70 km, respectively, and thus suggesting the acceleration of the mean zonal wind in response to the day-to-day variation of gravity wave activity. Using MLT wind data (2004–2010) acquired using MF Radar from Pameungpeuk (7.4°S, 107.4°E), Rao et al. (2012) found a strong correlation between the mesospheric semiannual oscillation and short period (20–120 min) gravity wave variances with enhanced Gravity wave activity during equinoxes when the mean zonal winds are primarily westward, thus suggesting the contribution of westward propagating gravity waves in imparting westward momentum to the zonal wind. Since the gravity wave variance alone is not sufficient enough to conclude wave-mean flow interaction, divergence of momentum fluxes, that is, zonal acceleration, is required. Antonita et al. (2008), using wind measurements for three continuous years (2004–2007) from meteor radar situated over Trivandrum (8.5°N, 76.9°E), reported the acceleration due to gravity wave momentum flux divergence to be ∼5–9 m/s/month and ∼−9 m/s/month in the 82–88 km altitude region during the westerly phase and the easterly phase of the MSAO, respectively, thus revealing seasonal variation in short period (2–3 hr) gravity wave momentum fluxes with equinoctial maximum and solstitial minimum. Moss et al. (2016) analyzed high-frequency gravity wave fluxes from mesospheric wind measurements using Ascension Island (8°S, 14°W) meteor radar and suggested that the westward acceleration imparted by high-frequency gravity waves is not always sufficient enough to drive the westward MSAO winds.

Primarily, gravity waves are localized mesoscale disturbances which are transient in nature and can provide efficient but localized eastward as well as westward forcings. Though planetary waves are mostly westward propagating waves, their amplitudes are less compared to diurnal tides and they are dominant during solstice months as well (Gurubaran et al., 2001 e.g.), when the mean winds are either eastward or relatively less westward. Migrating diurnal tides, on the other hand, can be described as a consistent wave phenomenon having a planetary scale horizontal wavelength and large westward momentum source. Suclupe et al. (2024) suggested the role of both DW1 tide and westward-propagating gravity waves in driving the abnormally strong westward winds during March equinox 2023 over low latitudes as a consequence of their momentum deposition. Using high-resolution (HR) WACCM-X model simulations, Krier et al. (2026) demonstrated how zonal forcing from the wave breaking of migrating diurnal tide could play a crucial role in driving the westward acceleration of the mean zonal winds from 80 to 100 km during the westward phase of the MSAO near March equinox over an equatorial region (15°S–15°N). Owing to the invariant and persistent nature of migrating diurnal tides, the novelty of our work lies in estimating the role of zonal acceleration (m/s/day) imparted by diurnal tides in driving the MSAO above 91 km at low latitudes (5°N–15°N) using ICON/MIGHTI winds for the first time. According to Killeen and Johnson (1995), upward propagating tides and gravity waves dissipate and deposit their energy and momentum into the background flow. In order to comprehend the role of solar diurnal tides on the mean background zonal flow, we need a quantitative understanding of momentum transport by dissipating solar diurnal tidal waves. Apart from the convergence of vertical flux of zonal momentum $\left(\frac{\partial}{\partial z}(< u'w' >)\right)$, which appears in the zonal acceleration equation, the vertical gradient of meridional flux of zonal momentum $\left(\frac{\partial}{\partial z}(< u'v' >)\right)$ is also considered owing to the symmetry in seasonal amplification of DTV with the mean westward winds for all 3 years. Diurnal tidal waves transport momentum as well as energy during their course of propagation. The amplitude grows exponentially with decreasing density, owing to energy conservation. However, this growth is restricted during tidal wave breaking at altitude levels where the deposition of eddy momentum flux becomes substantial. According to Lieberman and Hays (1994), the tidal damping causes redistribution of energy and momentum, thus defying the

Eliassen-Palm non-acceleration theorem resulting in the deposition of eddy momentum flux. This, in the case of solar diurnal tides, imparts semiannual westward acceleration within an altitude range of 95–100 km.

The results shown in our present study reveal that the westward acceleration induced by the vertical gradient of meridional flux of zonal momentum ($F_{\text{meridional}}$) due to diurnal tide exceeds the convergence of vertical flux of zonal momentum ($F_{\text{zonal}}$) due to diurnal tide from January to March around 97 km over the 3 years. This confirms the dominance of $F_{\text{meridional}}$ in driving the westward winds during these months, imparting a maximum westward acceleration of −43 m/s/day in March 2022. Compared to the zonal acceleration induced from January to March, larger westward acceleration is found to be induced by both $F_{\text{zonal}}$ and $F_{\text{meridional}}$ from August to November peaking in October (−55 m/s/day) in 2021. Using numerical experiments with the General Circulation Model, Lieberman and Hays (1994) noted westward diurnal tidal accelerations, ranging from −10 m/s/day to −60 m/s/day with corresponding mean zonal winds from −5 m/s to −30 m/s. They also reported westward acceleration close to −25 m/s/day calculated from the winds near 100 km observed from the space-borne HRDI instrument. Hines (1974) used Lindzen (1973)'s model results to reveal the zonal acceleration of −20 m/s/day imparted by the solar diurnal tides. The magnitude as well as the seasonal coherence observed between the westward acceleration (m/s/day) and the mean westward winds (m/s), exhibiting equinoctial maximum and solstitial minimum around 97 km, discernibly proves that momentum flux deposition by dissipation of migrating diurnal tides imparts adequate westward acceleration necessary in driving the MSAO from 95 to 100 km altitude region.

Compared to earlier studies showing different wave forcings driving the MSAO, the novelty in our work allows us to present a vivid seasonal picture quantifying the role of the zonal acceleration (m/s/day) induced by low latitude diurnal tides in both zonal and meridional winds derived from ICON/MIGHTI above 91 km in driving the mean zonal winds, for the first time. Thus, the results from our study, both qualitatively and quantitatively, emphasize how the momentum flux deposition by diurnal tides significantly contributes to driving the MSAO.

## 5. Summary and Conclusions

Using ICON/MIGHTI zonal and meridional winds, we not only demonstrate the seasonal variation of mean winds and tidal amplitudes in both zonal and meridional wind from 91 to 109 km within the region of interest (5° N–15°N, 63.5°E−90°E) for the years 2020, 2021 and 2022 but also highlight the role of diurnal tides in driving the mean zonal wind for the first time, in this study. The summary of the results are provided as follows:

1. Semiannual mean westward winds are found to dominate around 91–106 km with maximum intensity found at 97–100 km in February–March (−20 m/s to −43 m/s) and September–December (−24 m/s to −40 m/s).
2. In 2020 and 2021, we observe more intense westward winds from October to December compared to March at 97 km, whereas in 2022, maximum ICON/MIGHTI mean westward winds are captured during the month of March.
3. Similar semiannual variation of diurnal tidal amplitude in meridional wind (DTV) is found for all years, amplifying around 97–100 km in March (80 m/s to 100 m/s) and from November–December (75 m/s to 96 m/s).
4. DTU, though lacking a similar seasonal signature, is comparable to DTV in intensity and is found to be catalytic in westward wind amplification.
5. At higher altitudes (>103 km), strong semi-diurnal tidal amplitude in meridional wind (SDTV) persists for all years.
6. STDU, TDTU, and TDTV have relatively weaker magnitudes compared to DTU and DTV, and do not show any prominent seasonal variation.
7. The seasonal profiles of both $\phi_{\text{Meridional}}$ and $\phi_{\text{Zonal}}$ reveal characteristic downward phase progression with time, indicating upward diurnal tidal wave propagation.
8. The seasonal variation of westward acceleration derived from the deposition of zonal momentum flux of diurnal tides is found to be maximum from January to March (−18 m/s/day to −43 m/s/day) and from September to December (−40 m/s/day to −55 m/s/day) around 97–100 km and reveals similar semiannual variation as that of the mean westward winds with maximum intensity found at 97–100 km in February–March (−20 m/s to −43 m/s) and September–December (−24 m/s to −40 m/s) for all three years.
9. The westward acceleration induced by the vertical gradient of meridional flux of zonal momentum ($F_{\text{meridional}}$) shows a closer resemblance with the seasonal variation of westward winds than convergence of vertical flux of

zonal momentum ($F_{zonal}$) around 97 km altitude, for all years, thus indicating the significant role of momentum flux deposition of diurnal tides in driving the mean zonal flow.

10. $F_{meridional}$ exceeds $F_{zonal}$ explicitly from January to March in 2020 and 2021, which confirms the dominance of $F_{meridional}$ in driving the westward winds found during these months, imparting westward acceleration close to −18 m/s/day in March 2020 and −25 m/s/day in March 2021.

## Conflict of Interest

The authors declare no conflicts of interest relevant to this study.

## Availability Statement

The ICON/MIGHTI data products used in the present study are openly available and can be retrieved from the websites https://spdf.gsfc.nasa.gov/pub/data/icon/l2/l2-2_mighti_vector-wind-green/2019, https://spdf.gsfc.nasa.gov/pub/data/icon/l2/l2-2_mighti_vector-wind-green/2020, https://spdf.gsfc.nasa.gov/pub/data/icon/l2/l2-2_mighti_vector-wind-green/2021, https://spdf.gsfc.nasa.gov/pub/data/icon/l2/l2-2_mighti_vector-wind-green/2022. The density values are obtained from the instant run of NRLMSIS atmospheric model 2.0 from the website https://kauai.ccmc.gsfc.nasa.gov/instantrun/nrlmsis/.

**Acknowledgments**
The authors wish to thank the ICON data providers supported by NASA's Explorers Program and the ICON team working behind the instruments and data sets for making the data available in the public domain for the scientific community. This work has been supported by the Department of Space, Government of India.

## References

Akmaev, R. A., Forbes, J. M., & Hagan, M. E. (1996). Simulation of tides with a spectral mesosphere-lower thermosphere model. *Geophysical Research Letters*, *23*(16), 2173–2176. https://doi.org/10.1029/96GL01977

Andrews, D. G., Holton, J. R., & Leovy, C. B. (1987). *Middle atmosphere dynamics (No. 40)*. Academic Press. https://doi.org/10.1002/QJ.49711548612

Antonita, T. M., Ramkumar, G., Kumar, K. K., Appu, K. S., & Nambhoodiri, K. V. S. (2007). A quantitative study on the role of gravity waves in driving the tropical stratospheric semiannual oscillation. *Journal of Geophysical Research*, *112*(12), D12115. https://doi.org/10.1029/2006JD008250

Antonita, T. M., Ramkumar, G., Kumar, K. K., & Deepa, V. (2008). Meteor wind radar observations of gravity wave momentum fluxes and their forcing toward the mesospheric semiannual oscillation. *Journal of Geophysical Research*, *113*(10), D10115. https://doi.org/10.1029/2007JD009089

Beres, J. H., Garcia, R. R., Boville, B. A., & Sassi, F. (2005). Implementation of a gravity wave source spectrum parameterization dependent on the properties of convection in the Whole Atmosphere Community Climate Model (WACCM). *Journal of Geophysical Research*, *110*(D10), D10108. https://doi.org/10.1029/2004JD005504

Burrage, M. D., Vincent, R. A., Mayr, H. G., Skinner, W. R., Arnold, N. F., & Hays, P. B. (1996). Long-term variability in the equatorial middle atmosphere zonal wind. *Journal of Geophysical Research*, *101*(D8), 12847–12854. https://doi.org/10.1029/96JD00575

Chapman, S., & Lindzen, R. S. (1970). *Atmospheric tides: Thermal and gravitational* (p. 200). D. Reidel Press. https://doi.org/10.1007/978-94-010-3399-2

Deepa, V., Ramkumar, G., Antonita, M., Kumar, K. K., & Sasi, M. N. (2006). Vertical propagation characteristics and seasonal variability of tidal wind oscillations in the MLT region over Trivandrum (8.5°N, 77°E): First results from SKiYMET Meteor Radar. *Annals of Geophysics*, *24*(11), 2877–2889. https://doi.org/10.5194/angeo-24-2877-2006

Delisi, D. P., & Dunkerton, T. J. (1988). Seasonal variation of the semiannual oscillation. *Journal of the Atmospheric Sciences*, *45*(19), 2772–2787. https://doi.org/10.1175/1520-0469(1988)045<2772:SVOTSO>2.0.CO;2

Dunkerton, T. J. (1982). Theory of the mesopause semiannual oscillation. *Journal of the Atmospheric Sciences*, *39*(12), 2681–2690. https://doi.org/10.1175/1520-0469(1982)039<2681:TOTMSO>2.0.CO;2

Dutta, R., & Sridharan, S. (2023). Observational evidence for the influence of diurnal tide in driving winds in the polar upper mesosphere and lower thermosphere. *Journal of Geophysical Research: Space Physics*, *128*(3), e2022JA031104. https://doi.org/10.1029/2022JA031104

Emmert, J. T., Drob, D. P., Picone, J. M., Siskind, D. E., Jones, M., Jr., Mlynczak, M. G., et al. (2021). NRLMSIS 2.0: A whole-atmosphere empirical model of temperature and neutral species densities. *Earth and Space Science*, *8*(3), e2020EA001321. https://doi.org/10.1029/2020EA001321

Englert, C. R., Harlander, J. M., Marr, K. D., Harding, B. J., Makela, J. J., Fae, T., et al. (2023). Michelson Interferometer for Global High-Resolution Thermospheric Imaging (MIGHTI) on-orbit wind observations: Data analysis and instrument performance. *Space Science Reviews*, *219*(3), 27. https://doi.org/10.1007/s11214-023-00971-1

Eswaraiah, S., Ratnam, M. V., Murthy, B. V. K., Guharay, A., & Rao, S. V. B. (2013). Short period gravity wave momentum fluxes observed in the tropical troposphere, stratosphere and mesosphere. *Journal of Atmospheric and Solar-Terrestrial Physics*, *105–106*, 1–7. https://doi.org/10.1016/j.jastp.2013.07.001

Forbes, J. M., & Garrett, H. B. (1978). Thermal excitation of atmospheric tides due to insolation absorption by $O_3$ and $H_2O$. *Geophysical Research Letters*, *5*(12), 1013–1016. https://doi.org/10.1029/GL005i012p01013

Forbes, J. M., Oberheide, J., Zhang, X., Cullens, C., Englert, C. R., Harding, B. J., et al. (2022). Vertical coupling by solar semidiurnal tides in the thermosphere from ICON/MIGHTI measurements. *Journal of Geophysical Research: Space Physics*, *127*(5), e2022JA030288. https://doi.org/10.1029/2022JA030288

Fritts, D. C., & Vincent, R. A. (1987). Mesospheric momentum flux studies at Adelaide, Australia: Observations and a gravity wave–tidal interaction model. *Journal of the Atmospheric Sciences*, *44*(3), 605–619. https://doi.org/10.1175/1520-0469(1987)044

Gaikwad, H. P., Fadnavis, S., Gurav, O. B., Bhosale, J. L., Sharma, A. K., Patil, P. T., et al. (2023). The day-to-day variability in the mesosphere and lower thermosphere in low latitudes: A study using MF radar. *Advances in Space Research*, *71*(1), 199–215. https://doi.org/10.1016/j.asr.2022.08.066

Gao, H., Xu, J., Chen, G. M., Zhu, Y., He, M., Yuan, W., et al. (2024). Response of ICON/MIGHTI measured low-mid latitude OI630.0 and OI557.7 nm dayglow emissions to the 27 August 2021 geomagnetic storm. *Journal of Geophysical Research: Space Physics*, *129*(1), e2023JA032070. https://doi.org/10.1029/2023JA032070

Garcia, R. R. (2023). On the structure and variability of the migrating diurnal temperature tide observed by SABER. *Journal of the Atmospheric Sciences*, *80*(3), 687–704. https://doi.org/10.1175/JAS-D-22-0167.1

Garcia, R. R., Dunkerton, T. J., Lieberman, R. S., & Vincent, R. A. (1997). Climatology of the semiannual oscillation of the tropical middle atmosphere. *Journal of Geophysical Research*, *102*(D22), 26019–26032. https://doi.org/10.1029/97JD00207

Garcia, R. R., & Sassi, F. (1999). Modulation of the mesospheric semiannual oscillation by the quasibiennial oscillation. *Earth Planets and Space*, *51*(7–8), 563–569. https://doi.org/10.1186/BF03353215

Gurubaran, S., Sridharan, S., Ramkumar, T. K., & Rajaram, R. (2001). The mesospheric quasi-2-day wave over Tiruneveli (8.7°N). *Journal of Atmospheric and Solar-Terrestrial Physics*, *63*(10), 975–985. https://doi.org/10.1016/S1364-6826(01)00016-5

Hagan, M. E., Burrage, M. D., Forbes, J. M., Hackney, J., Randel, W. J., & Zhang, X. (1999). GSWM-98: Results for migrating solar tides. *Journal of Geophysical Research*, *104*(A4), 6813–6827. https://doi.org/10.1029/1998ja900125

Hines, C. O. (1974). Momentum deposition by atmospheric waves, and its effects on thermospheric circulation. *Geophysical Monograph Series*, *18*, 760–768. https://doi.org/10.1029/gm018p0760

Hines, C. O. (1997). Doppler-spread parameterization of gravity-wave momentum deposition in the middle atmosphere. Part 1: Basic formulation. *Journal of Atmospheric and Solar-Terrestrial Physics*, *59*(4), 371–386. https://doi.org/10.1016/S1364-6826(96)00079-X

Hitchman, M. H., Bywaters, K. W., Fritts, D. C., Coy, L. F., Kudeki, E., & Surucu, F. (1992). Mean winds and momentum fluxes over Jicamarca, Peru, during June and August 1987. *Journal of the Atmospheric Sciences*, *49*(24), 2371–2383. https://doi.org/10.1175/1520-0469(1992)049

Holton, J. R., & Wehrbein, W. M. (1980). A numerical model of the zonal mean circulation of the middle atmosphere. *PAGEOPH*, *118*(1), 284–306. https://doi.org/10.1007/BF01586455

Killeen, T. L., & Johnson, R. M. (1995). Upper atmospheric waves, turbulence, and winds: Importance for mesospheric and thermospheric studies. *Reviews of Geophysics*, *33*(1 S), 737–743. https://doi.org/10.1029/95RG00408

Krier, C. S., Liu, H., & Liu, G. (2026). Role of the diurnal tide in driving the westward phase of the mesospheric semiannual oscillation around March equinox. *Geophysical Research Letters*, *53*(3), e2025GL120218. https://doi.org/10.1029/2025GL120218

Li, M., Deng, Y., Harding, B. J., & England, S. (2024). Climatology of dayside E-region zonal neutral wind shears from ICON-MIGHTI observations. *Space Weather*, *22*(2), e2023SW003670. https://doi.org/10.1029/2023SW003670

Lieberman, R. S., Burrage, M. D., Gell, D. A., Hays, P. B., Marshall, A. R., Ortland, D. A., et al. (1993). Zonal mean winds in the equatorial mesosphere and lower thermosphere observed by the High Resolution Doppler Imager. *Geophysical Research Letters*, *20*(24), 2849–2852. https://doi.org/10.1029/93GL03120

Lieberman, R. S., & Hays, P. B. (1994). An estimate of the momentum deposition in the lower thermosphere by the observed diurnal tide. *Journal of the Atmospheric Sciences*, *51*(20), 3094–3105. https://doi.org/10.1175/1520-0469(1994)051<3094:AEOTMD>2.0.CO;2

Lindzen, R. S. (1973). Wave-mean flow interactions in the upper atmosphere. *Boundary-Layer Meteorology*, *4*(1–4), 327–343. https://doi.org/10.1007/BF02265242

Meenakshi, S., & Sridharan, S. (2024). Wavenumber-4 longitudinal structure in ICON-MIGHTI thermospheric meridional wind. *Journal of Geophysical Research: Space Physics*, *129*(6), e2024JA032642. https://doi.org/10.1029/2024JA032642

Mengel, J. G., Mayr, H. G., Chan, K. L., Hines, C. O., Reddy, C. A., Arnold, N. F., & Porter, H. S. (1995). Equatorial oscillations in the middle atmosphere generated by small scale gravity waves. *Geophysical Research Letters*, *22*(22), 3027–3030. https://doi.org/10.1029/95GL03059

Miyahara, S. (1981). Zonal mean winds induced by solar diurnal tides in the lower thermosphere. *Journal of the Meteorological Society of Japan. Series II*, *59*(3), 303–319. https://doi.org/10.2151/jmsj1965.59.3_303

Moss, A. C., Wright, C. J., Davis, R. N., & Mitchell, N. J. (2016). Gravity-wave momentum fluxes in the mesosphere over Ascension Island (8° S, 14° W) and the anomalous zonal winds of the semi-annual oscillation in 2002. *Annales Geophysicae*, *34*(2), 323–330. https://doi.org/10.5194/angeo-34-323-2016

Nakamura, T., Tsuda, T., Yamamoto, M., Fukao, S., & Kato, S. (1993). Characteristics of gravity waves in the mesosphere observed with the middle and upper atmosphere radar 1. Momentum flux. *Journal of Geophysical Research*, *98*(D5), 8899–8910. https://doi.org/10.1029/92JD02978

Rajaram, R., & Gurubaran, S. (1998). Seasonal variabilities of low-latitude mesospheric winds. *Annals of Geophysics*, *16*(2), 197–204. https://doi.org/10.1007/s00585-998-0197-4

Rao, N. V., Tsuda, T., & Kawatani, Y. (2012). A remarkable correlation between short period gravity waves and semiannual oscillation of the zonal wind in the equatorial mesopause region. *Annales Geophysicae*, *30*(4), 703–710. https://doi.org/10.5194/angeo-30-703-2012

Reed, R. J. (1966). Zonal wind behavior in the equatorial stratosphere and lower mesosphere. *Journal of Geophysical Research*, *71*(18), 4223–4233. https://doi.org/10.1029/JZ071i018p04223

Reid, I. M., & Vincent, R. A. (1987). Measurements of mesospheric gravity wave momentum fluxes and mean flow accelerations at Adelaide, Australia. *Journal of Atmospheric and Terrestrial Physics*, *49*(5), 443–460. https://doi.org/10.1016/0021-9169(87)90077-5

Richter, J. H., & Garcia, R. R. (2006). On the forcing of the mesospheric semi-annual oscillation in the whole atmosphere community climate model. *Geophysical Research Letters*, *33*(1), L01806. https://doi.org/10.1029/2005GL024378

Roble, R. G., & Ridley, E. C. (1994). A thermosphere-ionosphere-mesosphere-electrodynamics general circulation model (time-GCM): Equinox solar cycle minimum simulations (30–500 km). *Geophysical Research Letters*, *21*(6), 417–420. https://doi.org/10.1029/93GL03391

Sassi, F., & Garcia, R. R. (1997). The role of equatorial waves forced by convection in the tropical semi-annual oscillation. *Journal of the Atmospheric Sciences*, *54*(15), 1925–1942. https://doi.org/10.1175/1520-0469(1997)054<1925:TROEWF>2.0.CO;2

Sridharan, S. (2019). Seasonal variations of low-latitude migrating and nonmigrating diurnal and semidiurnal tides in TIMED-SABER temperature and their relationship with source variations. *Journal of Geophysical Research: Space Physics*, *124*(5), 3558–3572. https://doi.org/10.1029/2018JA026190

Sridharan, S. (2020). Equatorial upper mesospheric mean winds and tidal response to strong El Niño and La Niña. *Journal of Atmospheric and Solar-Terrestrial Physics*, *202*(2020), 105270. https://doi.org/10.1016/j.jastp.2020.105270

Sridharan, S., Tsuda, T., & Gurubaran, S. (2007). Radar observations of long-term variability of mesosphere and lowerthermosphere winds over Tirunelveli (8.7°N, 77.8°E). *Journal of Geophysical Research*, *112*(D23), D23105. https://doi.org/10.1029/2007JD008669

Suclupe, J., Chau, J. L., Conte, J. F., Pedatella, N. M., Garcia, R., Sato, K., et al. (2024). On the abnormally strong westward phase of the mesospheric semiannual oscillation at low latitudes during March equinox 2023. *Geophysical Research Letters*, *51*(16), e2024GL110331. https://doi.org/10.1029/2024GL110331

Suresh Babu, V., Ramkumar, G., & Rachel John, S. (2012). Seasonal variation of planetary wave momentum flux and the forcing towards mean flow acceleration in the MLT region. *Journal of Atmospheric and Solar-Terrestrial Physics*, *78–79*, 53–61. https://doi.org/10.1016/j.jastp.2011.05.010

Teitelbaum, H., & Vial, F. (1981). Momentum transfer to the thermosphere by atmospheric tides. *Journal of Geophysical Research*, *86*(C10), 9693–9697. https://doi.org/10.1029/jc086ic10p09693

Teja, A. K., Ratnam, M. V., & Rao, S. V. B. (2024). Mean winds and tidal variability from troposphere to the thermosphere retrieved from combined ground based and space borne measurements. *Journal of Atmospheric and Solar-Terrestrial Physics*, *265*, 106389. https://doi.org/10.1016/j.jastp.2024.106389

Tomikawa, Y., Sato, K., Watanabe, S., Kawatani, Y., Miyazaki, K., & Takahashi, M. (2008). Wintertime temperature maximum at the subtropical stratopause in a T213l256 GCM. *Journal of Geophysical Research*, *113*(D17), D17117. https://doi.org/10.1029/2008jd009786

Vincent, R. A., & Reid, I. M. (1983). HF Doppler measurements of mesospheric gravity wave momentum fluxes. *Journal of the Atmospheric Sciences*, *40*(5), 1321–1333. https://doi.org/10.1175/1520-0469(1983)040

Yamazaki, Y., Harding, B. J., Qiu, L., Stolle, C., Siddiqui, T. A., Miyoshi, Y., et al. (2023). Monthly climatologies of zonal-mean and tidal winds in the thermosphere as observed by ICON/MIGHTI during April 2020–March 2022. *Earth and Space Science*, *10*(6), e2023EA002962. https://doi.org/10.1029/2023EA002962

Yiğit, E., Dhadly, M., Medvedev, A. S., Harding, B. J., Englert, C. R., Wu, Q., & Immel, T. J. (2022). Characterization of the thermospheric mean winds and circulation during solstice using ICON/MIGHTI observations. *Journal of Geophysical Research: Space Physics*, *127*(11), e2022JA030851. https://doi.org/10.1029/2022JA030851

Zhang, S. P., McLandress, C., & Shepherd, G. G. (2007). Satellite observations of mean winds and tides in the lower thermosphere: 2. Wind Imaging Interferometer monthly winds for 1992 and 1993. *Journal of Geophysical Research*, *112*(21), D21105. https://doi.org/10.1029/2007JD008457